Structure and Properties of Tin-Containing Polymers Deposited from Tetramethyltin HF Plasma

T. H. YING, A. M. SARMADI,* C. E. C. A. HOP, and F. DENES

Department of Environment, Textiles and Design, Department of Chemistry and Engineering Research Center for Plasma-Aided Manufacturing, University of Wisconsin-Madison, Madison, Wisconsin 53706

SYNOPSIS

There has been an increasing interest in depositing metal or metal-containing thin films through plasma polymerization for various applications. This work deals with the plasma graft polymerization of tetramethyltin (TMT) on polypropylene surfaces with an aim of producing special electrical and optical coatings. The fragmentation of TMT under cold plasma conditions and the recombination of discharge-generated active species were studied by analyzing the resulting molecular mixture trapped outside of the plasma zone by HR-MS and GC-MS techniques. It was found that the predominant ionic fragment is m/z = 165, and the most probable intermediate structure of the polymer formation mechanism is hexamethylditin. The structure of polymeric layers deposited on various substrates were investigated by ESCA and FT-IR methods. Intense oxidation of tin-based polymeric layers were observed under open laboratory conditions. The existence of weak Sn–Sn and Sn–C bonds in the polymeric structures is suggested to be responsible for this reaction. This phenomenon was associated with enhanced UV transparency. Based on analytical data a plasma-enhanced polymerization mechanism of TMT is proposed. © 1995 John Wiley & Sons, Inc.

INTRODUCTION

Volatile organometallic compounds can be converted into solid polymeric films under cold plasma conditions.[1-3] Depending on the experimental parameters, metal or metal-containing polymer depositions can be achieved. These layers can exhibit mirrorlike (metallic) or opaque appearances, and their electric conductivity can be in the ranges of insulators, semiconductors, or conductors. Their transparency in certain wavelength domains of the electromagnetic spectrum suggest for optical applications [e.g., ultraviolet (UV) filters, transparent heating elements, etc.). Some of these films can selectively retain various gases like CO, propane, water vapors, etc., and modify accordingly their electric conductivity. These phenomena open up possibilities for designing low- and high-temperature gas sensor devices. Metal and metal-containing polymer depositions can also be considered in applications where corrosion resistance is required. Antistatic and antireflective coatings enlarge the field of application of these materials.

Although extensive work has been reported on plasma-enhanced tin and tin-containing polymer depositions, little data is available on the mechanism of film formation (plasma-induced molecular fragmentation and active species recombination into solid phase networks on substrate surfaces) and on the stability of these layers under open laboratory conditions. Suhr and coworkers prepared thin metallic tin films by plasma technique from tetramethyltin (TMT) and from mixtures of TMT with argon and hydrogen under various experimental conditions.[4] In the presence of oxygen, carbon disappears almost completely and the films become semiconducting and transparent. It was established that extraneous depolymerization gas (O_2) must not be added to get films with metallic properties. By controlling the main parameters (power density, sub-

* To whom correspondence should be addressed.

Journal of Applied Polymer Science, Vol. 55, 1537–1551 (1995)
 CCC 0021-8995/95/111537-15

strate temperature, and monomer flow or partial pressure of starting components), it was possible to deposit either metallic films or metal–polymer films of different composition. The influence of plasma parameters on the tin content of the polymers and on their electrical resistivity was also investigated. Inagaki and coworkers[5–8] studied the glow discharge polymerization of the pure TMT and its mixtures with methane, acetylene, and nitrogen and of tin acetylacetonate dichloride. Their research emphasized that TMT is more easily polymerized than methane, and its deposition rate was comparable to that of tetramethylsilane (TMS). The methane and acetylene contents of the gas mixtures have a significant influence on the carbon and tin atoms incorporated into the polymeric structures. Compared to TMT-originated plasma polymers where the carbon and tin contents represent about 44 and 27 percentages, respectively, plasma polymers resulted from TMT and methane and TMT and acetylene mixtures, with equal molar ratios, exhibit a much lower carbon content (20%) and a significantly higher tin content (60–70%). These results are unusual because higher C/Sn ratio mixtures led to lower C/Sn ratio based polymers. Plasma polymers resulted from methane and acetylene exhibit usually a very high carbon content.

The authors do not provide a mechanism to explain this phenomenon. The polymers from these mixtures are built up mainly from CH_3, CH_2, CH, Sn—O, and Sn—O—Sn entities. They also found that the presence of nitrogen in the starting mixture induced amino group formation. Surface energy, UV, and visible absorption characteristics and thermal stability of polymeric layers were investigated as well. These investigations also exhibit data on adhesion behavior between plasma films and polymer substrates and on gas sensitivity parameters of plasma films for flammable gases such as carbon monoxide, ethanol, hydrogen, and methane. Kny and co-workers[9–11] studied the composition, interface composition, and adhesion of organo-tin polymer films from metallic substrate materials. The X-ray photoelectron spectroscopy (XPS) and atomic emission spectroscopy (AES) origin X-ray beam and electron impact effects on the atomic composition of plasma films were established and analyzed in detail in their investigation. Based on the carbon-to-tin ratio values, an atomic polymerization mechanism was suggested. It was demonstrated that the nature of the substrate material and its position in the discharge have a significant influence on the composition of the films and the presence of a sandwich-type interfacial structure was evidenced (e.g., $Al/Al_2O_3/Sn$ oxides/carbon-rich structure). These investigations emphasize that the TMT-based polymeric films are semiconductors, having conductivity values between the limits of 2×10^{-1} and 1×10^{-2} ohm^{-1} cm^{-1}. The influence of an electron beam and of thermal treatment on the electrical properties of tin-containing polymers were also discussed. Angadi and co-workers,[12] and Yamada and co-worker[13] studied the effect of the deposition rate on the electrical resistivity and etching resistance of plasma-polymerized tin films, while Chen and coworkers[14] analyzed their electrochemical behavior. Sadhir and co-worker[1–3,15] demonstrated that mirrorlike metallic tin, thin (1000 Å) films can be synthesized by simultaneously introducing TMT and oxygen into a glow discharge. They found that the flow rate of oxygen plays a significant role in the rate of deposition of the films, and high values of this parameter induce surface ablation reactions. The TMT-based films showed a sheet conductivity in the range of about 10^2–10^4 ohm^{-1} cm^{-1}. A carbon-to-tin ratio of less than 2 of the surface layers was found necessary to achieve a conducting film. Electron diffraction and X-ray diffraction spectra of the films indicate the presence of β-Sn structure. The films were stable under ambient conditions, but temperatures higher than 63°C increased their conductivity irreversibly. The polymeric layers adhere strongly to metals, ceramics, composites, and plastics and are good water vapor barriers.

In this work the mechanism of TMT-based film formation in an HF plasma is examined and the properties of polymeric layers are discussed.

EXPERIMENTAL

Materials and Methods

Tetramethyltin (Aldrich) and hexamethylditin (Sterm Chemicals, Inc.) were used in all of the experiments as received. Both chemicals were handled in a glove box under an argon blanket. Heavy-duty aluminum foil was used to cover the parallel plate electrodes in order to avoid direct deposition of polymers on the electrodes and to facilitate the cleaning problems. Optically smooth quartz (1 × 1 inch, Suprasil 1, Heraus Amersil Inc.) and glass (1 × 1 inch, Fisher Scientific Co.) windows, potassium bromide pellets (13 mm diameter, FT-IR grade, Aldrich), aluminum foil, and polypropylene (PP) fabrics (Test Fabrics, Inc.) were selected as substrates. High-purity argon (liquid carbonic) was used to clean the reactor before each experiment.

The infrared (IR) spectra of the Sn-containing polymeric layers deposited on KBr pellets were recorded on a Mattson Galaxy Series FTIR-5000 instrument under 4 cm^{-1} resolution. The measurements were carried out under moisture and CO_2-free Ar atmosphere.

The surface atomic composition of tin-based polymeric films was analyzed using X-ray photoelectron spectroscopy (ESCA, Perkin-Elmer Physical Electronics O 5400 Small Area System; Mg source; 15 kV, 300 W; pass energy: 35.750 eV; angle: 15°). The ESCA analysis involved the determination of carbon (C_{1s}), tin (Sn_{3d3}, Sn_{3d5}, and oxygen (O_{1s}). All samples were stored under vacuum conditions until the measurements were started; this limited moisture absorption processes and oxidation reactions.

The complex mixture of neutral molecules and active species (free radicals, ions, etc.) were collected for analytical purposes, in a specially designed stainless steel liquid nitrogen trap (Fig. 1). Valves [1] and [2] permitted the isolation of volatile compounds under vacuum conditions and a chromatography-type septum [3] assured the proper sampling for gas chromatography–mass spectrometry (GC–MS) analysis by means of a Hamilton gas syringe. The outer diameter (6 mm) of the connecting stainless steel tubing [5], matched the dimensions of the connection of the inlet line of the high-resolution (HR) MS, providing vacuum-proof connecting possibilities.

The chemical compounds resulting from the recombination in the trap of plasma-generated active species were investigated by using a GC–MS (GC–Carlo Erba Fractovap 4162; MS Kratos MS-25; experimental conditions: column-fused silica, length 30 m, ID 0.32 mm, coating 0.25 μm of 5% phenyl and 95% vinyl polysiloxane, injector–splitter temperature 25°C, temperature profile of column 5 min at room temperature then heated up to 250°C at

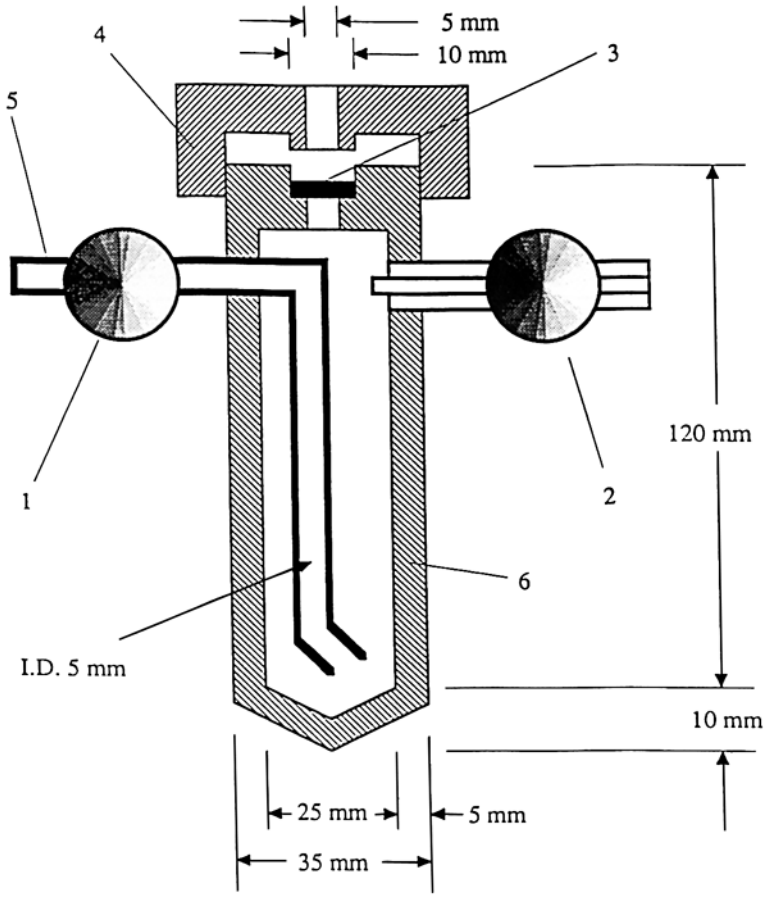

Figure 1 Stainless steel trap designed to collect the plasma-generated compounds at liquid nitrogen temperature: (1,2) needle valves; (3) chromatography type septum, (4) stainless steel trap; (5) stainless steel connecting tubing (O.D. = 5 mm); (6) stainless steel cylindrical body of the trap).

15°C/min, electron energy 28 eV) and a HR-MS (Kratos MS-80, electron energy 50 eV). Both MS instruments are double focusing mass spectrometers (electrostatic analyzer and magnet) provided with electron impact ion source. The HR–MS spectra were recorded by connecting the stainless steel trap directly to the spectrometer; the admission valve was opened after evacuating the connecting lines.

The transparency in the UV range of the original and oxidized films, deposited on optically smooth quartz windows were monitored by employing an HP B452A Diode Array Spectrophotometer and a Perkin–Elmer Coleman 55 Spectrophotometer. The thicknesses of the polymeric layers were established by using a interferometer.

Plasma Reactions

The plasma-enhanced experiments were carried out in a parallel plate stainless steel cylindrical reactor (Fig. 2) with an electrode diameter of 20 cm and spacing of 3 cm. The upper electrode [15] was connected to a matching network and a RF generator (30 KHz), and the lower electrode [22] was grounded. The upper electrode and the base plate of the reactor [28] were cooled to avoid extensive heating and to avoid damaging the electronic components located below the reactor. The substrates were placed on the lower electrode [22] which was provided with a heating element [17] in order to monitor the influence of the substrate temperature on the atomic

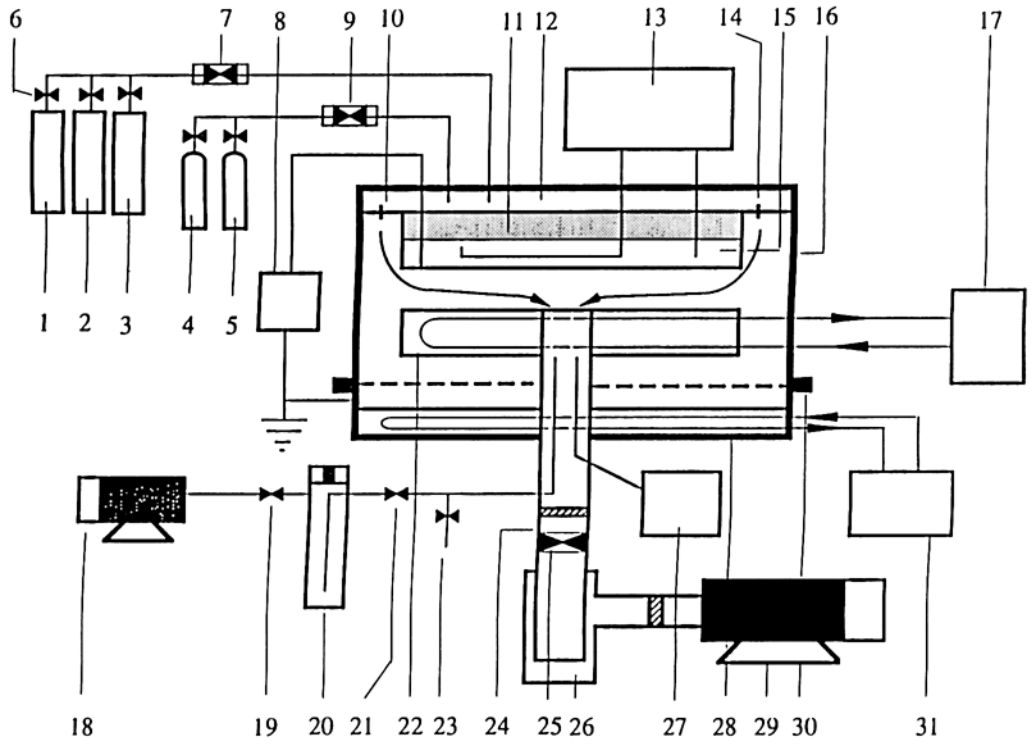

Figure 2 Parallel plate RF cold plasma installation: (1,2,3) monomer reservoirs; (4) argon reservoir; (5) CF_4 reservoir; (6,19,21,23) stainless steel needle valves; (8) HF generator; (7,9) flow controllers; (10,14) monomer and/or gas inlet orifices, located circularly around the upper electrode (shower type feeding); (11) electric insulator disc; (12) gas mixing chamber; (13) programmable refrigerated circulator; (15) drum-type stainless steel upper electrode; (16) cylindrically shaped upper part of reactor; (17) temperature controller for the built-in electric heater of the lower electrode; (18) mechanical vacuum pump; (20) stainless steel liquid nitrogen trap for collecting the plasma-generated molecular mixture; (22) grounded lower stainless steel electrode; (24) 1-inch diameter stainless steel connecting tubing; (25) large cross section butterfly-type valve; (26) stainless steel liquid nitrogen trap for protecting vacuum pump; (27) vacuum gauge; (28) drum-type stainless steel lower part of the reactor; (29) high-capacity mechanical vacuum pump; (30) rubber O-ring mediated circular vacuum tight sealing; (31) refrigerated recirculator.

composition of the plasma polymers. The reactor was equipped with two vacuum lines connected by means of 1-inch stainless steel tubing [24] to the reaction chamber and positioned through the center of the lower electrode. In this way the gas flow penetrates symmetrically into the discharge zone located between the electrodes. One of the vacuum lines composed of large cross-section valve [25], liquid nitrogen trap [26], and high-capacity vacuum pump [29] assured the quick evacuation of the reactor to the base pressure level and pump oil flashback during the experiments and the protection of the pump from chemical contamination. At the same time, valve [25] permitted equilibrium conditions to be established between the incoming and outgoing flow rates. The second vacuum system composed of stainless steel needle valves [19,21,23], specially designed liquid nitrogen trap [20], and mechanical vacuum pump [18] equipped with its own liquid nitrogen trap (not shown in Fig. 2) assured the collection and trapping of plasma-generated active species and neutrals for analytical purposes. Needle valve [23] was used as a vent. Each experiment was preceded by a cleaning operation in the absence of substrates, in order to remove possible low-volatility contaminants from earlier experiment. The cleaning procedure involved igniting the discharge in a CF_4 environment (flow rate 11 sccm; pressure 300 mTorr, RF power 200 W) for 5 min, followed by argon plasma discharge under the same conditions. Both the lower and the upper electrodes were covered with aluminum foil (heavy-duty brand, Reynolds) before each experiment, to facilitate cleaning up procedures. The substrates were optically smooth glass and quartz slides, aluminum foil, KBr pellets, and polypropylene (PP) fabrics positioned symmetrically versus the center of the electrode. The vapors of TMT and hexamethyldisiloxane (HMDSO) were introduced from monomer reservoirs [1 and 2] through different leak valves and from flow controller [7] at the desired flow rates. The monomers were degassed by freezing them at liquid nitrogen temperature, vacuumed to ground pressure level, and isolated by closing the corresponding needle valves [6]. During the experiments the monomer reservoirs were kept at room temperature.

In a typical experiment after the selected substrates were positioned on the aluminum-covered lower electrode, the upper part of the reactor was locked and the system was evacuated through an open valve [25] with the aid of high-capacity vacuum pump [29]. The second vacuum line also was operated, but it was isolated from the system by closed valves [21 and 23]. Both traps were cooled down using liquid nitrogen. After reaching the ground pressure level the selected temperatures for the electrodes were established and a flow meter [7] was opened to evacuate the connecting stainless steel tubing. Then the flow meter was closed and the monomer valve [6] was opened. By operating the valve of flow meter and valve [25] the selected pressure and flow rate were established in the reactor at a equilibrium rate. The plasma was then ignited and the discharge was sustained for the required time period. At the plasma's ignition moment valves [19 and 21] were opened for trapping the plasma-generated species. After completion of the selected trapping time period, the second vacuum line and the trap were isolated from the system by closing valves [19 and 21]. At the end of the reaction the RF power was disconnected, flow meters and monomer feeding valves were closed, valve [25] was completely opened, and the system was evacuated to ground pressure level. Vent valve [23] was then opened and the reactor was opened by translating its upper part, and the samples were quickly placed in vacuum desiccator and stored for analytical purposes. Trap [20] was also removed from the system and stored for GC–MS and HR–MS measurements. The experimental conditions used during the plasma treatments were as follows:

Monomer: TMT, HMDSO
RF power: 20 W
Ground pressure: 120 mTorr
Pressure in the absence of plasma: 200 mTorr
Pressure in the presence of plasma: 220 mTorr
Temperature of the substrate holder: 20, 60, 80, 100, and 120°C
Monomer flow rate: 11 sccm
Trapping period: 1 min
Treatment time: 1, 3, 5, 8, and 10 min

RESULTS AND DISCUSSIONS

The weight gain monitored on optically smooth quartz windows versus treatment time shows a linear relationship (Fig. 3). This behavior indicates that a steady-state condition has been established between the deposition and ablation reactions during the 10 min reaction time interval. Similar polymer accumulation patterns were noticed in the cases of glass, polypropylene, and aluminum substrates. Thickness estimations were performed interferometrically in all cases by collecting data from five different lo-

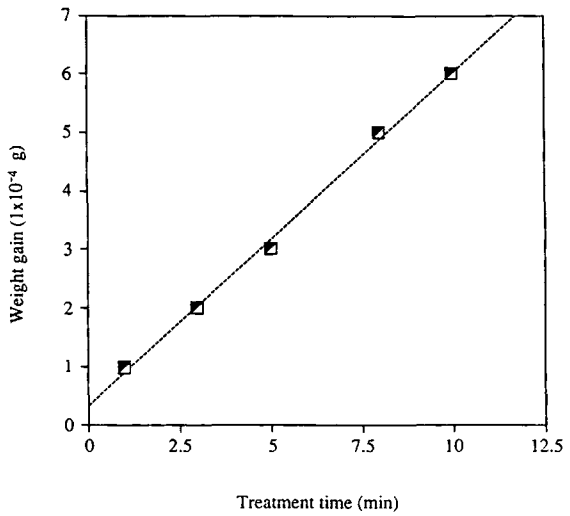

Figure 3 Influence of plasma treatment time on the weight gain of PTMT (Substrate: 1X inch optically smooth quartz window; thickness estimations were performed interferometrically by collecting data from five different locations of the substrate).

cations of the substrates. However, the physical aspects (transparency, color, smoothness, etc.) of the polymeric layers deposited on various substrates were strikingly different. Vinogradov[16] recently found that well-defined experimental conditions of plasma–surface interactions evidently demonstrate the direct influences of electric fields on the kinetics of heterogeneous plasma chemical processes in a near surface area of a solid body being in contact with plasma. Additional experimental data are required on tin-based plasma–polymer depositions to learn more on the influence of dielectric properties of various substrates on the structure of these compounds.

FTIR spectroscopy represents an important technique for investigation of organotin compounds. It is noteworthy that almost all of the stretching vibrations involving the tin atom occur at wavenumbers below 650 cm^{-1}. Conventional IR windows (NaCl, KBr, etc.) are opaque below 400 cm^{-1}, leaving only a narrow vibrational range for investigation. This is likely why it is rather difficult to correctly assign of Sn–C and Sn—O vibrations. Another complication arises from the fact that the positions of these vibrations are sensitive to changes in coordination number of tin atom, to the electronegativity of the substients, to the size and the nature of the alkyl subsistent, and to the physical state of the sample.[16] The weak Sn—O—Sn vibrations in the ranges of 780–770 cm^{-1} and around 400 cm^{-1}, due to the linearity of the system, are also difficult to assign, and Sn—Sn asymmetrical vibrations (in the symmetrically substituted distannanes the Sn—Sn mode is IR inactive) present below 200 cm^{-1} require special windows (CsI or high-density polyethylene). The sensitivity to oxygen of tin-based derivatives and especially of tin-containing polymers synthesized by plasma techniques (the presence of free radicals) makes IR analyses even more difficult. Table I shows some of the assignments for Sn—C and Sn—O vibrations based on literature data, and

Table I Literature Data Based IR Assignments for Sn—C; Sn—O and Sn—Sn Bonds

Frequencies	Wavenumber (cm^{-1}) 1000	900	800	700	600	500	400	300	200	Ref.
Sn—C stretching (alkyl comp). √asym. √sym.					■	■				21
Sn–ethynil rocking				■			■			
Sn–methynil rocking			■							
Sn—O stretching					■	■		■		
Sn—OH def		■								
(alkyl)x, Sn—OH; COOH; O; CO_3		■	■		■	■				
Sn—O—Sn				■		■		■		
Sn—O—C	■									
Sn—Sn									■	
PTMT polymer										
Sn—C			■		■	■				2
Sn—O					■		■			5
Sn—Sn									■	4, 10
Sn—H: 1180 cm^{-1}										

emphasizes the frequent superimposition of assigned regions for these two different vibrations.

The time-dependent oxidation of plasma-polymerized TMT (PTMT) polymers would permit the proper assignment of Sn—O and Sn—C vibration by monitoring the appearance or intensification and disappearance or diminuation of certain vibrations in the Sn-associated absorption ranges.

Figure 4 exhibits a typical FTIR spectrum of a PTMT polymer and Figure 5 shows the FTIR spectra of a PTMT polymer stored under open laboratory conditions, and recorded at different time interval in the 500–900 cm^{-1} wavenumber range. Polymers prepared from TMT show absorptions at 2950, 2900, 1465, and 1385 cm^{-1} due to CH_3, CH_2, and CH groups and a relatively strong absorption around 3500 cm^{-1} that is peculiar to OH functional groups (Fig. 4). An increasing OH–CN_x ratio (Table II) versus elapsed time can be noticed when the samples are stored under open laboratory conditions (conditioning room; temperature 25°C; relative humidity 65%). Literature data present different opinion on oxygen and hydroxides from tin surfaces. The existence of structures varying from pure stanneous oxide[17,18] to mixtures of anhydrous stanneous oxide and $Sn(OH)_2$ and $Sn(OH)_4$ hydroxides were suggested.[19–20]

The presence of three major absorptions (723, 569, and 511 cm^{-1}) can be remarked in the high-resolution FTIR spectrum of PTMT recorded in the wavelength number interval of 500–900 cm^{-1} (Fig. 5). It is clear that frequency vibrations corresponding to 723 and 569 cm^{-1} wavenumbers diminish and finally disappear at higher elapsed time values; meanwhile the weak shoulder from 764 cm^{-1} gradually becomes a major peak in the same time interval. A slight upward absorption shift corresponding to 511 cm^{-1} wavenumber is also evident. These time-dependent modifications developed in the presence of air can be explained by the disappearance of some of the Sn—C bonds (723, 569 cm^{-1}) and the formation of Sn—O—linkages (764 cm^{-1}) through oxidation mechanisms. The Sn–Sn bond scission from the —C—Sn—Sn—C— structure, under moisture and oxygen-containing atmosphere conditions, certainly would result in Sn—O bond generation and also in Sn—C bond scission. This possible mechanism would consequently result in the decrease in Sn—C bond content and in the formation of C—O and unsaturated linkages. Formation of ketone,

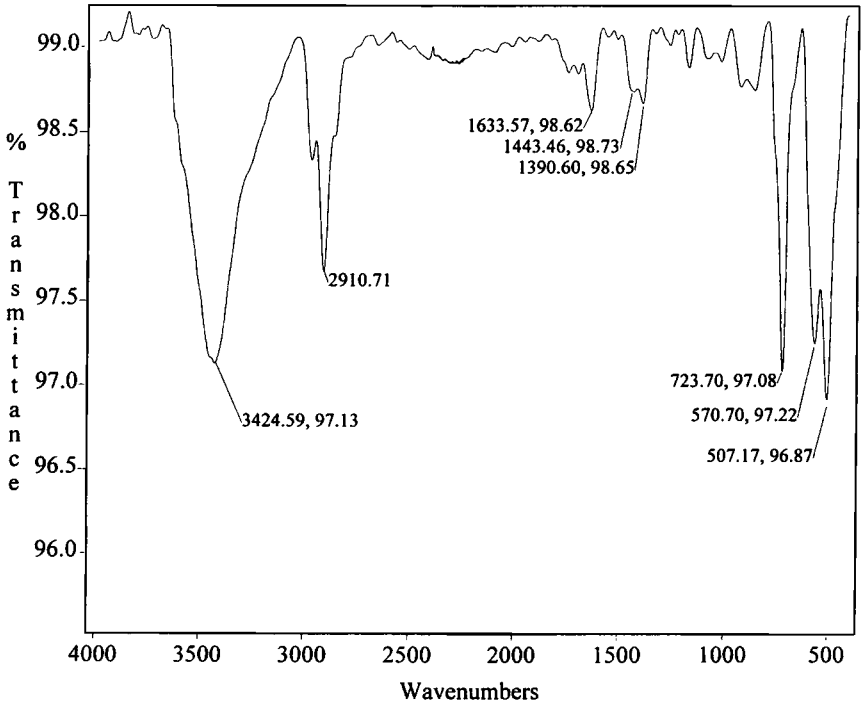

Figure 4 General FTIR spectrum of PTMT, recoded from PTMT directly deposited under RF–TMT plasma conditions (temperature of substrate holder 20°C, deposition time 1 min) on KBr pellet substrates.

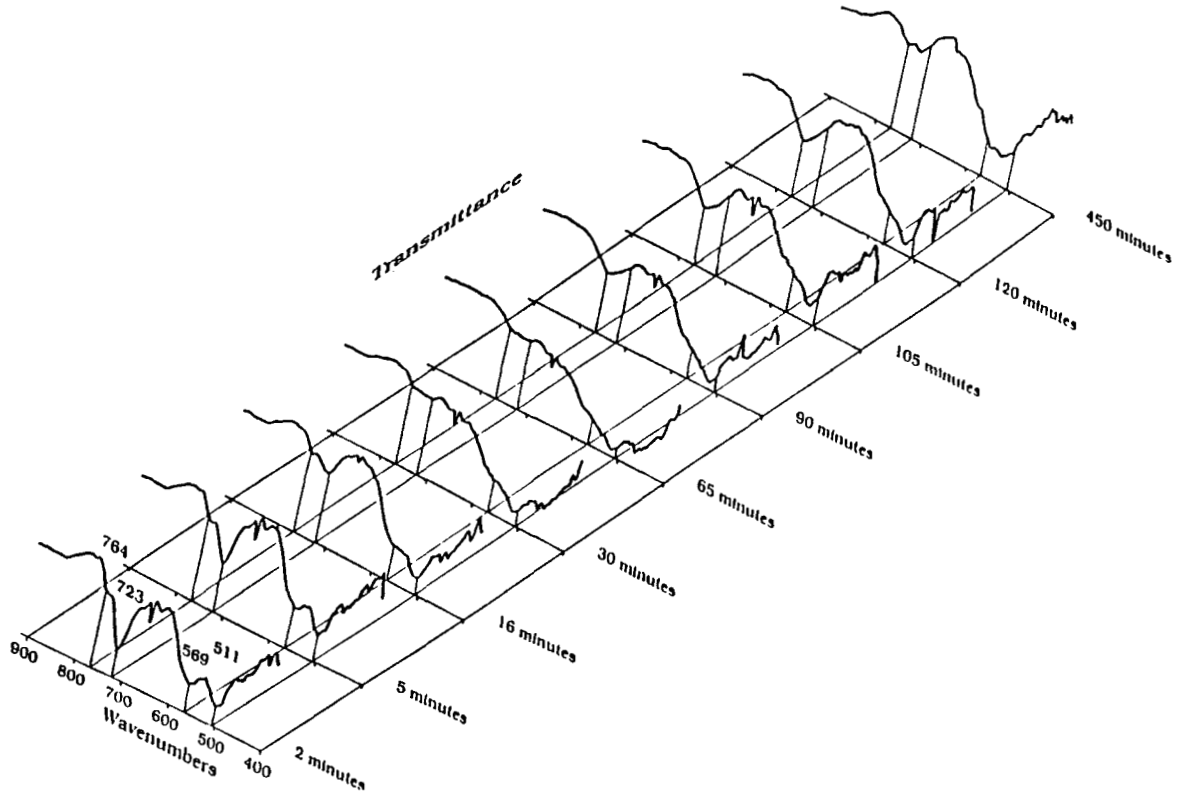

Figure 5 Influence of storing period, under open laboratory conditions (conditioning room: temperature 25°C; relative humidity 65%), on the FTIR spectra patterns (oxidation) in the 400–900 wavenumber range.

peroxide, ether, and hydroxyl groups from plasma-generated free-radical-containing structures are also possible. However, the 1720–1750 cm-1 and 100–1200 cm-1 regions do not exhibit major absorptions. The shift of absorption 511 cm^{-1} on the wavenumber scale probably reflects molecular reorganizations.

ESCA measurements bring information on the atomic composition of the PTMT polymers. High-resolution ESCA estimation of carbon (Fig. 6) and tin (Fig. 7) regions exhibit the existence of a symmetrical C_{1s} peak (285 eV) associated with a low-intensity satelite (288.5 eV) generated probably by the formation of oxygen- and carbon-based linkages, and the doublet character of the tin-based diagram. The existence of an oxidized C_{12} peak can be explained through postplasma oxidation processes during handling. The influence of target temperature on the surface atomic composition of the Sn-based polymeric layers in the 20–100°C temperature range (the temperature interval within textile fabrics are usually processes) is presented in Table III. A high tin and oxygen content can be remarked in all of the cases. It is also noteworthy that the temperature of the substrate does not significantly influence the surface atomic composition values below 100°C. Fairly intense oxidation can be noticed in all the cases.

UV spectroscopy data collected from PTMT polymers deposited on optically smooth quartz windows are in good agreement with FTIR and ESCA results. Oxidation reaction mediated enhanced UV transparency can be remarked. Figure 8 shows the

Table II Ratio of OH–CHx[a] Estimated from PTMT Data

Elapsed Time (min)	Ratio
2	4.35
5	4.59
16	5.28
30	5.34
90	7.23
120	7.67
450	10.67
1440	15.37

[a] OH–CH*x* functional group ratio estimations were carried out by integrating the areas of 3424 and 2910 cm^{-1} peaks (Fig. 4) of the same sample at various elapsed times.

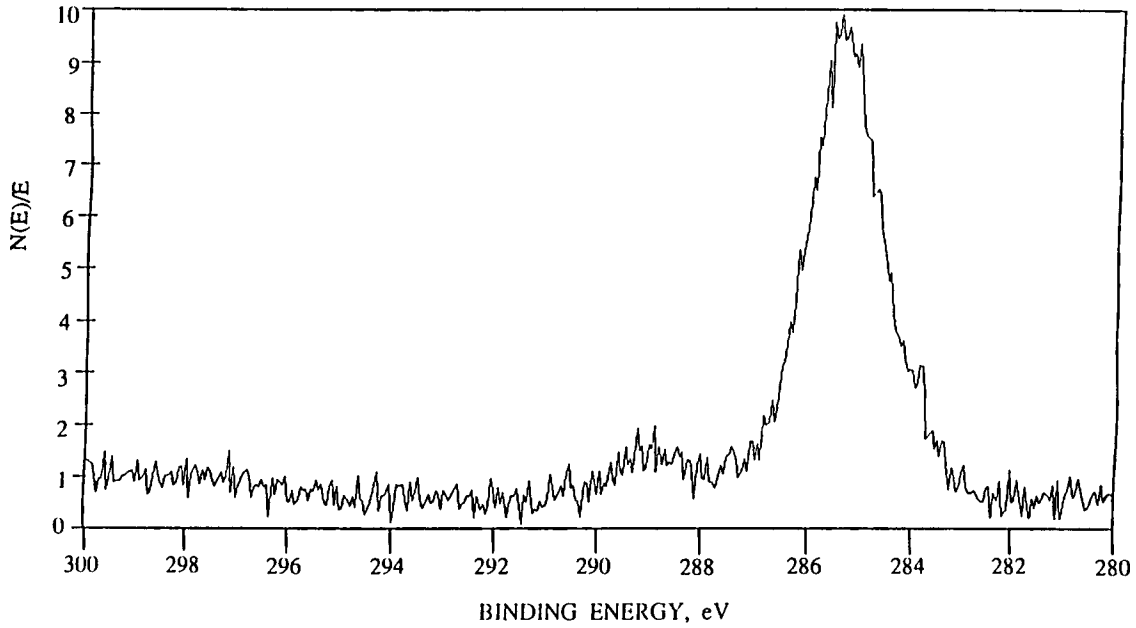

Figure 6 Detailed C_{1s} ESCA spectrum from PTMT.

comparative UV–visible spectra of a typical PTMT polymer recorded at two different elapsed time values. Higher transparency values occur when a sample is exposed to atmospheric conditions for a longer time period. Since the deposited films are thin layers, oxygen and moisture penetration through a diffusion mechanism would also affect the bulk structure of the polymers. More accurate measurements carried out in the 325–385 nm region (Fig. 9), at various exposure time intervals show about a 40% transparency change in 15 h. After 250 min 95% of the highest transparency value is reached (Fig. 10), which corresponds fairly well with the oxidation-reaction-determined weight gain modifications (Fig. 11). Films deposited from HMDSO under similar conditions present no such phenomenon (Fig. 12).

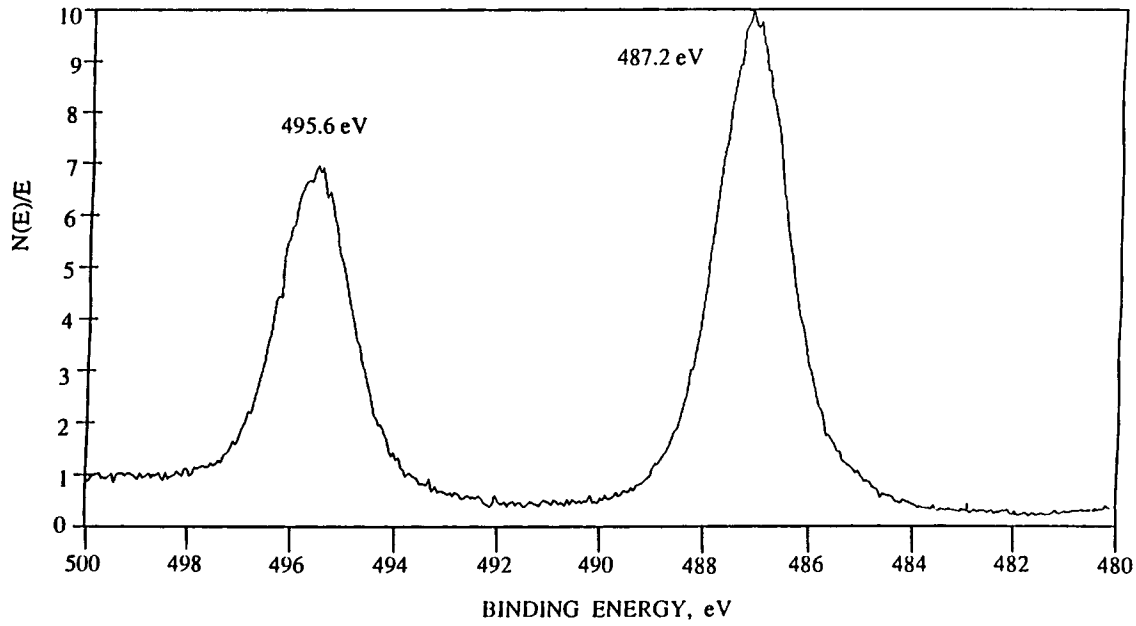

Figure 7 Detailed Sn_{3d3} and Sn_{3d5} ESCA spectrum from PTMT.

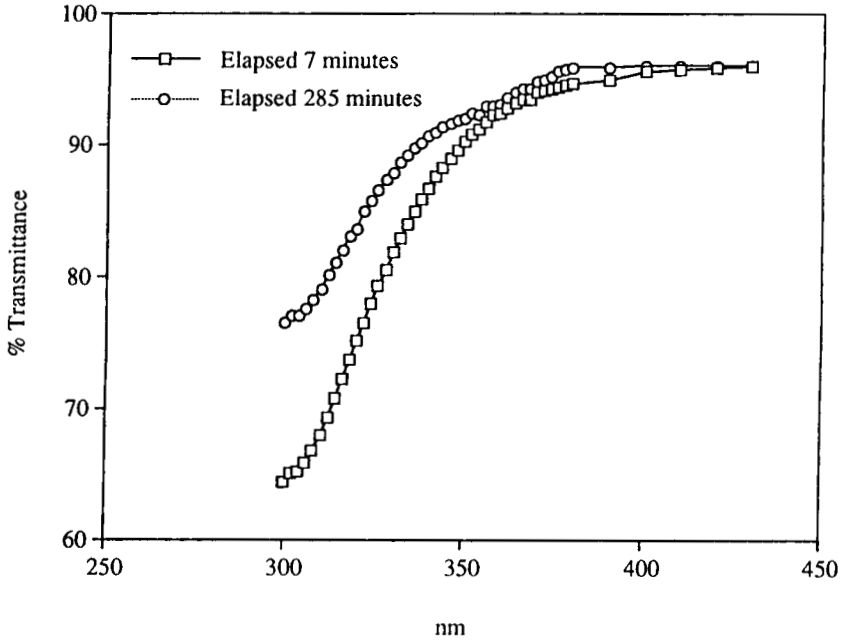

Figure 8 Influence of oxidation on UV transparency from PTMT thin films recorded from quartz windows at two different elapsed times.

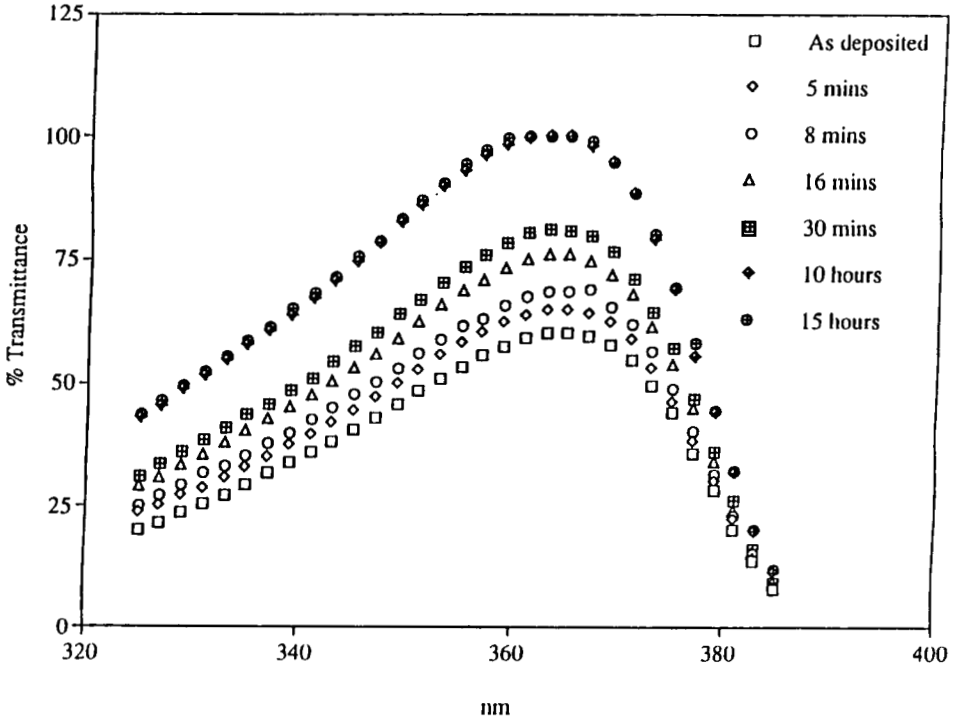

Figure 9 Oxidation-induced UV transparency monitored at $\lambda = 325$ nm, at various elapsed time values from the deposition (open laboratory conditions).

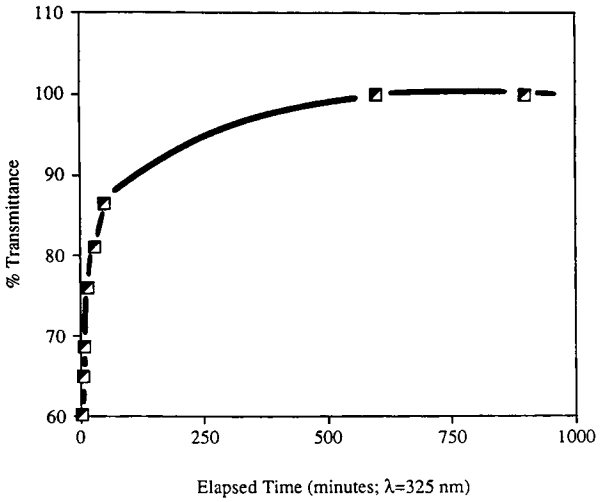

Figure 10 Influence of elapsed time on UV transparency (λ = 325 nm).

Significant modifications in the transparency values are not evident even at long exposure. This behavior is important because it opens up possibilities for using very thin PHMDSO layers to protect different UV-transparency PTMT structures. Practical applications for UV filters can also be considered on this way.

HR–MS data of standard TMT (Fig. 13) carried out at 50-eV electron energy indicate that the most significant fragmentation process is demethylation

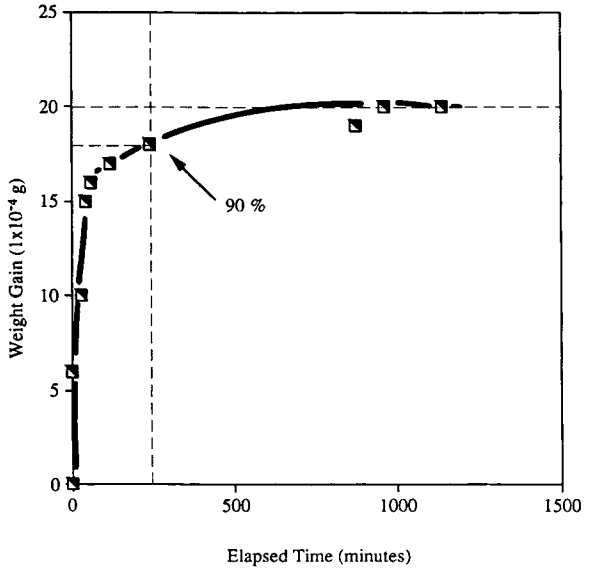

Figure 11 Influence of elapsed time on the weight gain of PTMT (the measurements were carried out under conditioning room environment: temperature 25°C, relative humidity 65%).

and that the predominant ionic fragment is m/z = 165. The clusters grouped around m/z = 165 ($Sn(CH_3)_3^+$), m/z = 150 ($Sn(CH_3)_2^+$), m/z = 135 ($Sn(CH_3)^+$), and m/z = 120 (Sn) reflect the isotopic composition of Sn only. Consequently recombination processes developed on the surfaces which limit the plasma or on surfaces outside of the discharge zone (e.g., cold trap) would result in important hexamethylditin (HMDT) formation, provided the plasma conditions mimic the conditions in the ion source of the MS. Certainly the deposited structures in contact with the plasma state would undergo further modifications. Figure 14 shows the HR–MS spectrum of the mixture of TMT and HMDT (electron energy 50 eV). The fragmentation pattern of HMDT is practically similar with that of TMT. The weakness of the Sn–Sn bond (46 Kcal/mol) is responsible for this phenomenon. The energy of the ionizing electrons is utilized mainly for Sn–Sn bond cleavage mechanisms. The plasma-induced HMDT formation can be proved, however, by separating the trapped components based on their volatility in a GC and recording their MS spectra. Figure 15 presents the GC profile (GC–MS method) of the molecular mixture (gaseous phase fraction from the liquid nitrogen trap) resulting from the recombination of plasma-generated active species. Figures 16 and 17 show the comparative MS spectra (gaseous phase components) of the two major GC peaks. It clearly can be noticed that the GC peaks correspond to similar MS fragmentation patterns; this indicates both the presence of unreacted TMT and the existence of plasma-generated HMDT. When using ether as a solvent, the liquid phase compounds collected from the cold trap were also analyzed by GC–MS technique. Data were recorded similar to that in the case of gaseous phase samples; m/z values around 120, 135, 150, and 165 were the only ionic fragments both in the cases of lower and higher re-

Table III Relative Atomic Composition of PTMT, Estimated by Polymer ESCA Technique Synthesized at Different Temperatures of Substrate

	Atomic Concentration (%)		
Sub. Temp.	Carbon	Oxygen	Tin
Room	41	36	23
60°C	43	36	21
80°C	44	36	20
100°C	35	40	25

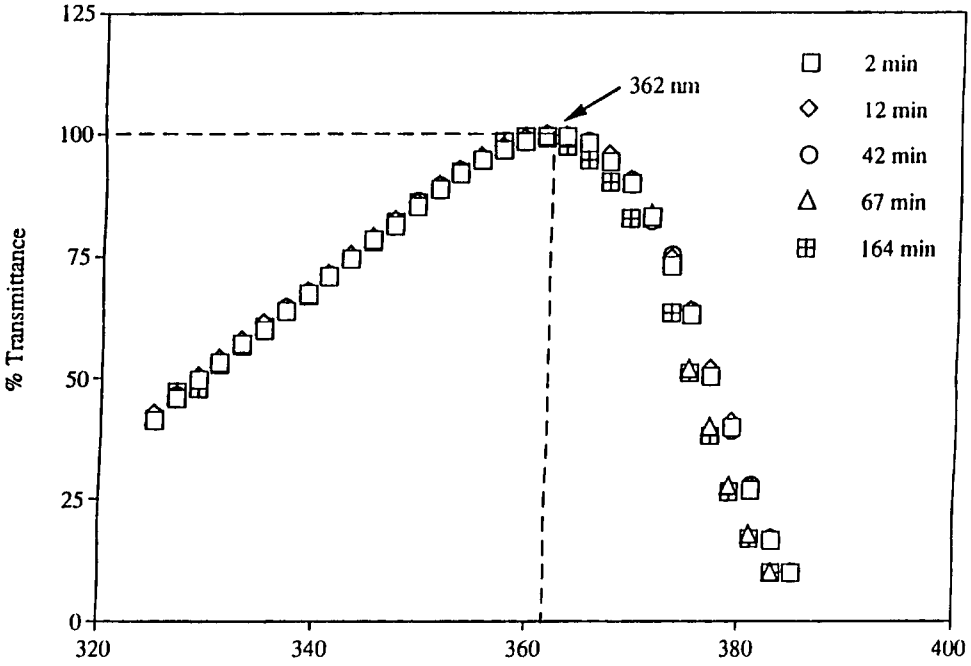

Figure 12 Influence of elapsed time (open laboratory conditions) on the UV transparency of PHMDSO film, deposited on optically smooth quartz window.

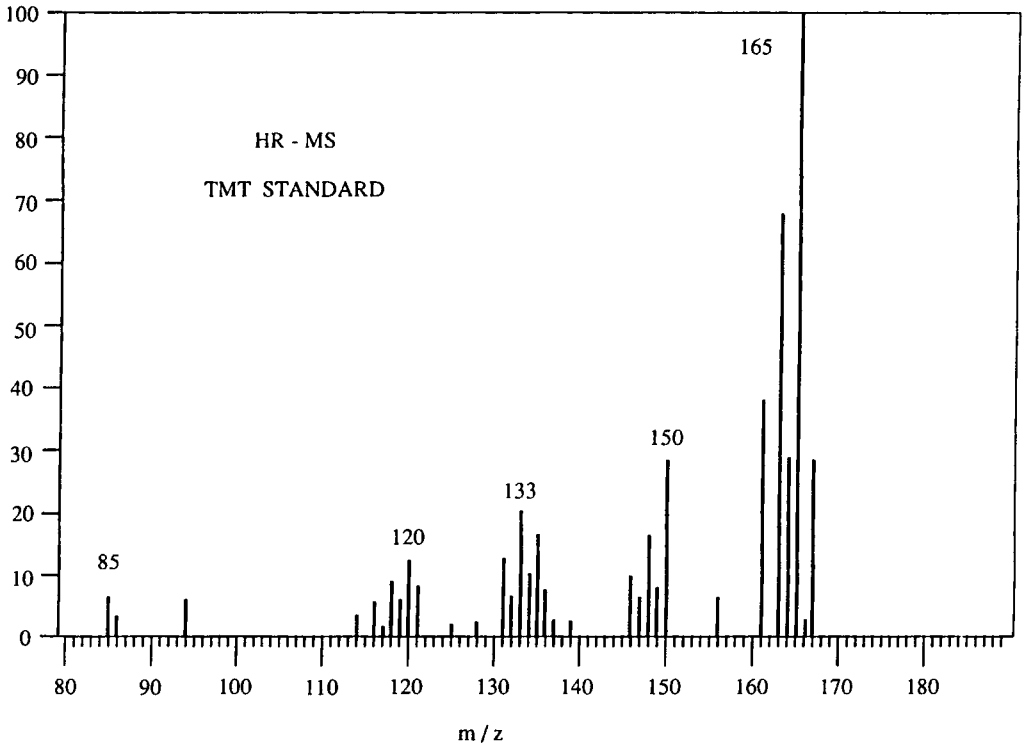

Figure 13 Standard HR–MS spectrum of TMT.

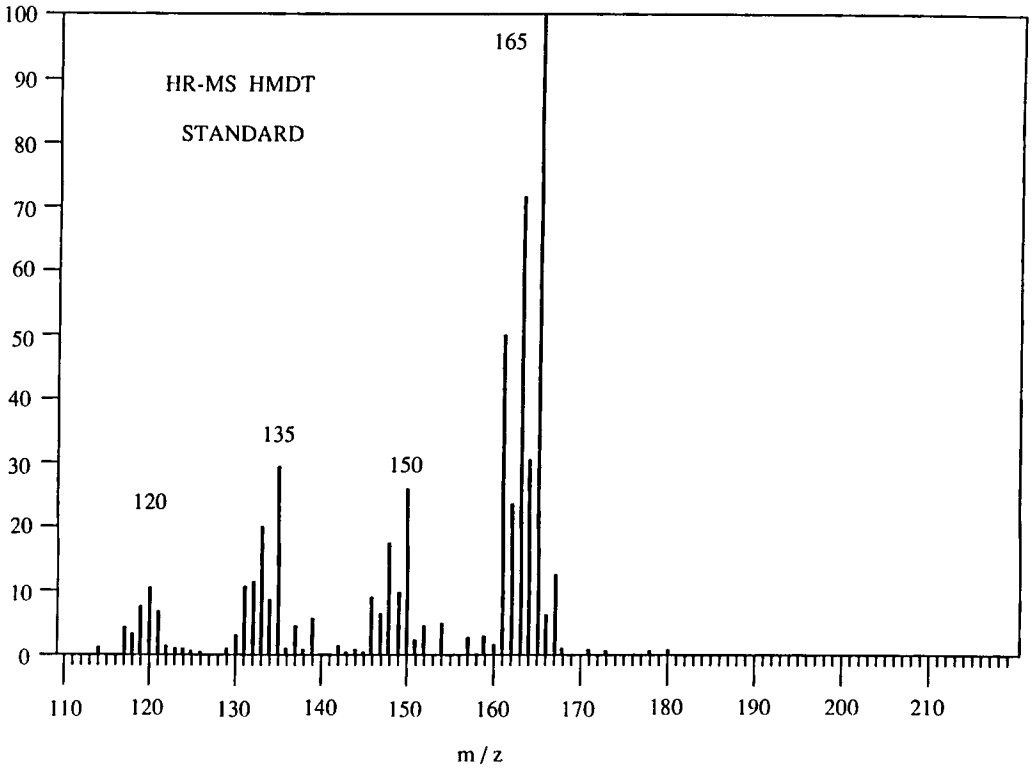

Figure 14 Standard HR–MS spectrum of HMDT.

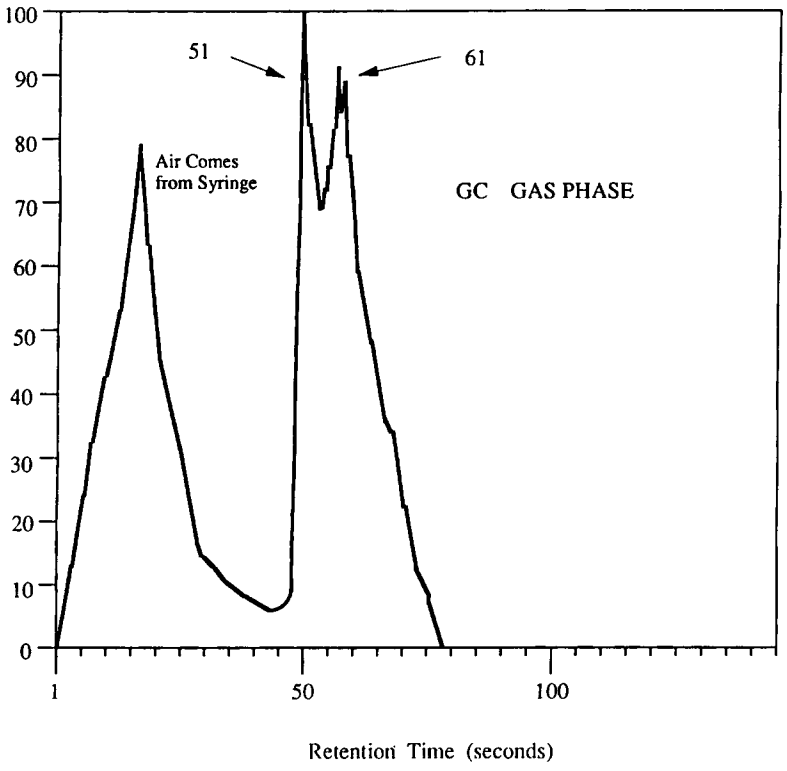

Figure 15 Gas chromatography of gaseous phase fraction of plasma-generated molecular mixture, collected in liquid nitrogen trap.

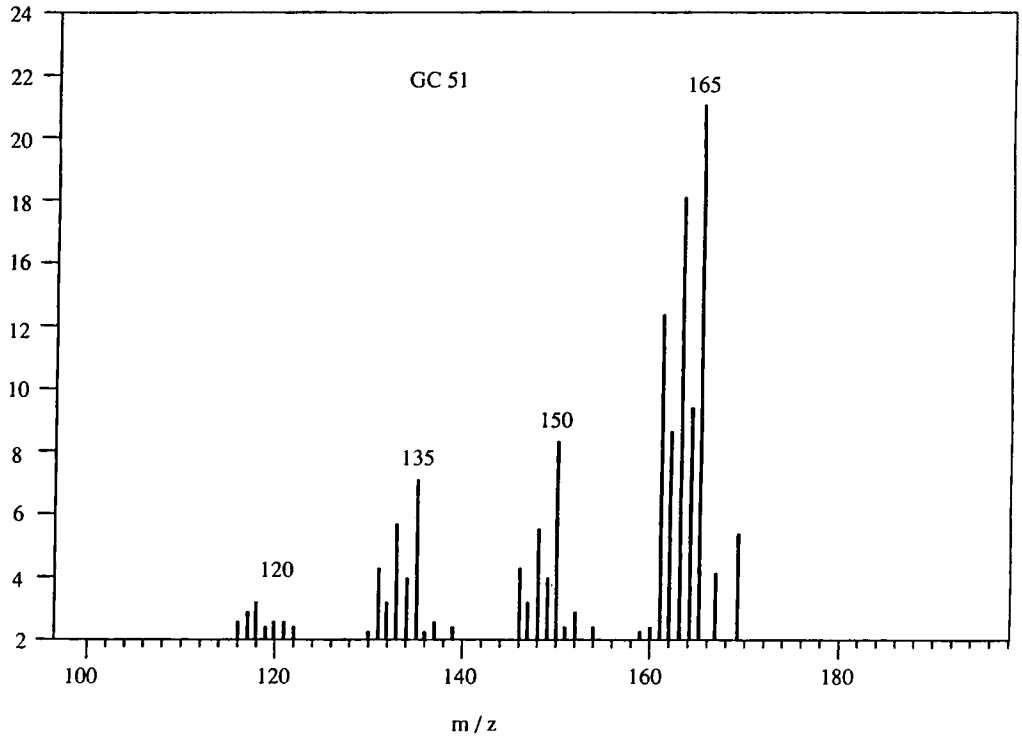

Figure 16 Low-energy electron (LEE)–MS spectrum of GC fraction 51.

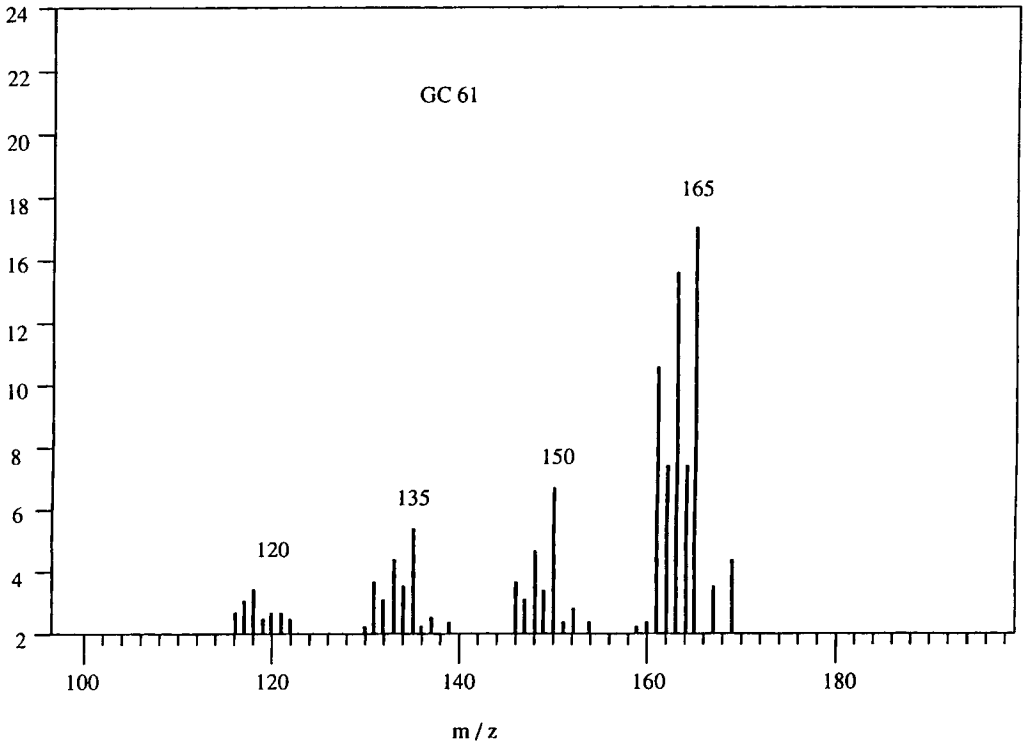

Figure 17 LEE–MS spectrum of GC fraction 61.

tention time major GC peaks. These data suggest that HMDT is the main intermediate derivative adsorbed on the substrate surfaces during TMT plasma treatments. Due to the presence of dehydrogenation processes which accompany both the plasma and MS electron-induced TMT fragmentation, the formation of higher molecular weight structures through recombination and crosslinking mechanisms can not be excluded. Their low volatility, however, limit their detection and identification. This structure will undergo further modifications under the action of active species of plasma (e.g., dehydrogenation, demethylation, crosslinking) leading eventually to the formation of Sn-based polymeric layers. It is noteworthy that not even *in situ* MS measurements would detect the presence of HMDT-type structures; identification requires separation so as to understand the plasma-induced fragmentation and recombination reactions.

CONCLUSIONS

1. Different nature substrates can easily be coated with thin polymeric layers with metallic appearances from a TMT RF plasma.
2. PTMT polymers deposited on various substrates exhibit different morphological appearances (metal-like, mirrorlike, transparent, colored, etc.). Further studies are required in order to understand the influence of the nature of the substrate on the structure of plasma-generated thin polymeric layers.
3. FTIR and ESCA analyses of the deposited polymeric layers indicate the presence of a Sn—C and Sn—O based structure. The Sn—O linkages were generated through post-plasma oxidation processes under open laboratory conditions. During the oxidation reactions the deposited polymeric layer became partly transparent and/or colored (yellow-blueish).
4. ESCA measurements show that the atomic composition of TMT polymers are not affected significantly by the temperature of the substrate in the range of 20–120°C.
5. The oxidation reactions are associated with enhanced UV transparency of the polymeric layers. By depositing thin HMDSO layers over PTMT films, the oxidation reaction intensity was shown to be controllable; consequently different UV transparency levels are possible and UV filter designs are considered.
6. GC—NS and HR–MS data obtained from the trapped molecular mixture obtained from the recombining plasma-generated active species indicate that the main ionic fragment in plasma is m/z = 165 (demethylated TMT), and HMDT is suggested as the principal molecular intermediate in the polymer forming process. These structures adsorbed on substrate surfaces undergo further modifications (dehydrogenation, demethylation reactions) under the action of active species of plasma and transform into polymeric networks through recombination processes.

REFERENCES

1. R. K. Sadhir and H. E. Saunders, *J. Vac. Sci. Technol.*, **A3**(6), 2093 (1985).
2. N. Inagaki, S. Tasaka, and K. Suzuki, *Proc. ACS Div. Polym. Mater.: Sci. Eng.*, **62,** 543 (1990).
3. H. Suhr, A. Etspuler, E. Feurer, and C. Oehr, *Plasma Chem. Plasma Proc,* **8,** 9 (1988).
4. C. Oehr and H. Suhr, *Thin Solid Films,* **155,** 65 (1987).
5. N. Inagaki, T. Yagi, and K. Katsuura, *Eur. Polym. J.*, **18,** 621 (1982).
6. N. Inagaki, T. Nishio, and K. Katsuura, *J. Polym. Sci.: Polym. Lett. Ed.*, **18,** 765 (1980).
7. N. Inagaki and Y. Hashimoto, *Polym. Mater. Sci. Eng.*, **62,** 543 (1990).
8. N. Inagaki, S. Tasaka, and K. Suzuki, *J. Appl. Polym. Sci.: Appl. Polym. Symp.*, **46,** 173 (1990).
9. E. Kny, L. L. Levenson, and W. J. James, *Thin Solid Films,* **64,** 395 (1979).
10. E. Kny, L. L. Levenson, and W. J. James, *J. Vac. Sci. Technol.*, **16**(2), 359 (1979).
11. E. Kny, L. L. Levenson, W. J. James, and R. A. Auerbach, *Thin Solid Films,* **85,** 23 (1981).
12. M. A. Angadi and L. A. Udachan, *Thin Solid Films,* **78,** 299 (1981).
13. H. Yamada, T. Satoh, S. Itoh, M. Hori, M. Nakamura, S. Morita, and S. Hattori, *J. Vac. Sci. Technol,* **B7**(2), 175 (1989).
14. Y. M. Chen, T. J. O'Keefe, and W. J. James, *Thin Solid Films,* **129,** 205 (1985).
15. R. K. Sadhir and W. J. James, *Thin Solid Films,* **97,** 17 (1982).
16. G. K. Vinogradov, *Proc. ISPC, London,* 1559 (1993).
17. J. Yang, *Disc. Faraday Soc.*, **1,** 196 (1947).
18. F. W. Salt and J. G. N. Thomas, *Nature (London),* **178,** 434 (1956).
19. C. O. Bannister, *J. Tust, Met.*, **35,** 71 (1926).
20. S. E. S. El Wakland, T. M. Salem, and J. A. El Sayed, *J. Chem. Soc.*, 3770 (1957).
21. R. C. Poller, *The Chemistry of Organotin Compounds,* Logos Press, London, 1970.

Received April 12, 1994
Accepted September 19, 1994